Salt concentration effects on evaporation-driven pattern formation in sessile droplets

Cécile Lalanne, Anaëlle Givaudan, Paul Boumendil, Florence Lequien, José-Maria Fullana

Salt concentration effects on evaporation-driven pattern formation in sessile droplets

Cécile Lalanne[a,b], Anaëlle Givaudan[b], Paul Boumendil[b], Florence Lequien[a], José-Maria Fullana[b]

[a] *Université Paris-Saclay, CEA, Service de recherche en Corrosion et Comportement des Matériaux, 91191 Gif Sur Yvette, France*
[b] *Sorbonne Université, CNRS, UMR 7190, Institut Jean Le Rond d'Alembert, Paris, France*

Abstract

We report experimental findings on the formation of salt deposits upon the complete evaporation of a sessile droplet containing sodium chloride. We also offer both quantitative and qualitative information to help comprehend the intricate mechanisms underlying the evaporation problem.

We propose a mechanism for solutal instability that aligns with our experimental results and literature findings. During the solute crystallization and eventual deposit formation, we observe two phases: the first phase, where crystal growth is absent, spans from the initial time to 65 % of the evaporation duration. The second phase occurs when the chemical process of crystallization sets in. We provide quantitative data on the crystallization process, utilizing the normalized average distance between crystals as a function of relative humidity and initial salt concentration.

Keywords: sessile droplet, evaporation, salt stains, instability, Marangoni

*Corresponding author
Email address: jose.fullana@sorbonne-universite.fr (José-Maria Fullana)

1. Introduction

Accurately predicting and comprehending pattern formation resulting from dried sessile droplets is critical for various industrial applications, including ink printing [1], film coating [2], metal corrosion [3], particle self-assembly, and bio-medicine [4]. The formation of salt deposits described in the literature depends mainly on the initial solute concentration and the external evaporation conditions [5].

When a sessile droplet containing non-volatile solutes evaporates, a variety of patterns may form, such as the well-known coffee-ring and uniform stains [6]. The deposition patterns that arise on the solid substrate after complete droplet evaporation result from the intricate hydrodynamic and chemical mechanisms occurring during the evaporation process [7, 8]. By understanding the flows inside the droplet, we can explain the dried patterns, as Deegan did for the ring-stain in his pioneering work [6]. Previous studies have explored the density and dynamics of non-volatile particles contained in the solution during evaporation, highlighting the complexity of the mechanisms underlying the formation of dried patterns (sse the review of [5]).

For small sessile droplets of density ρ, surface tension γ, radius r under gravity g with a Bond number $Bo = \frac{\rho g}{\gamma} r^2 << 1$, if the contact angle runs between 0 and 90 $^\circ$, the evaporation flux is larger at the triple contact line than at the top of the droplet. The unbalanced evaporation flux is then compensated by an internal fluid flow from the center to the edge of the droplet, and where the solvent lost by evaporation has to be replenished to ensure the spherical-cap shape of the droplet. This primary mechanism brings besides

the fluid from the center to the triple line transporting all particles present in the solution giving the coffee-ring deposition. Hu and Larson [9]shows that the thermal Marangoni effect cancels the coffee-ring deposition by a recirculatory flow driven by surface-tension gradients produced by the latent heat of evaporation. For sessile droplets containing sodium chloride the surface tension increases with salt concentration, leading to local variations of surface tension. In some particular conditions when the surface tension gradient is large enough, a solutal Marangoni flow takes place along the droplet interface [10, 11]. The solutal Marangoni flow for intermediate sodium chloride concentration suppress also the coffee-ring deposition giving an uniform pattern [7]. The solutal Marangoni flow, a secondary mechanism, contributes therefore to the rise of solute concentration near the triple contact line and this will eventually result in crystallization if the critical salt concentration is exceeded. The effect of sodium chloride concentration on the evaporation dynamics and particles motion has been also analyzed in [12, 13].

When droplets containing sodium chloride concentrations evaporate, nucleation and crystal growth occur under specific external conditions that are not yet fully understood. Nucleation occurs at high solute concentrations, which can be reached after a certain evaporation time depending on various factors, such as initial solute concentration, evaporation conditions, and droplet size.

While the final location of crystals near or at the triple contact line where the solute concentration is high appears coherent, the quantity and spatial arrangement of crystals obtained after the evaporation of a saline sessile droplet under different relative humidities are not yet fully explained. In

references [14, 7, 15] the authors put forward arguments of trans-reservoir instability to explain the structures observed, but we believe that in our configuration, instabilities of this type, triggered by surface tension, are also at the origin of the deposits. This suggests the presence of an instability mechanism, as other complex structures in the deposit pattern are also attributed to hydrodynamic instability [16].

For instance, the fingering phenomenon is explained by the competition between the outward capillary flow and the inward Marangoni flow. The relative humidity of the environment around the droplet is a crucial parameter that affects the evaporation dynamics and the total time of evaporation. Therefore, relative humidity is a factor that can influence the final deposit pattern [17].

This study aims to experimentally investigate the evaporation of saline sessile droplets and analyze the impact of relative humidity on the crystalline deposits. The paper analyzes the final structures by examining the wavelength between salt crystals and proposes an instability mechanism to explain the quantity, shape, and location of the crystals.

2. Experimental set-up

In the experiment, a saline sessile droplet is placed inside a laboratory glove box with a controlled humidity device (W-Tech), as shown in Figure 1..

The glove box has a volume of 250 L and the relative humidity (RH) can be adjusted from 5% to 50%, while the temperature inside the glove box remains constant at 25.0 $^{\circ}$C. Both temperature and humidity are continuously

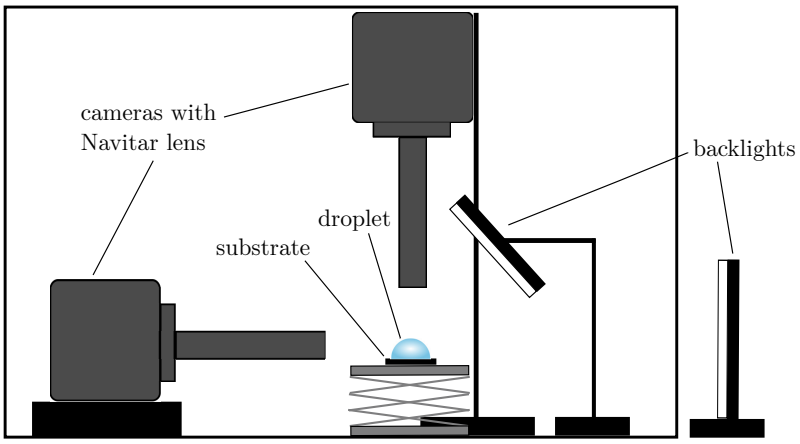

Figure 1: Schematic illustration of the experimental set-up inside the laboratory glove box.

monitored and kept constant during each experiment. The air around the droplet is assumed to be at rest, and since the typical size of the glove box (1 m) is much larger than the typical length of the droplet radius (around 10^{-3} m), convective flows are neglected.

The sessile droplet is deposited by a micropipette onto a solid substrate, a silicon wafer (SIL'TRONIX Silicon Technologies). The silicon wafer is single-sided polished, with a surface roughness less than 5 A rms. We use a high precision micropipette to form sessile droplets of controlled volumes from 10 to 100 μL. The saline solutions are prepared with Sodium Chloride NaCl (Sigma Aldrich) with salt concentrations ranging from 10^{-4} to 1.5 $mol.L^{-1}$ NaCl. We start with a solution with the maximum salt concentration of 1.5 $mol.L^{-1}$ NaCl and by dilution in distilled water we can reach small salt concentrations. Some blue dye (e133) is added to the solutions to improve the view of the crystals at the end of the evaporation process. The amount is small and does not alter the properties of the solution. Nikon D810 cameras

equipped with a Navitar lens record the evaporation dynamics simultaneously images every 15 seconds from two sides. In order to capture high-quality photos, the setup is illuminated from both the side and the top using two backlights, positioned both inside and outside the glove box.

Figure 2 presents typical data collected over the experiences. The side view allows the continuous monitoring of the shape dynamics by measuring the contact angle, the droplet height and the contact radius (Figure 2(a)). It also enables to study the crystals emergence as shown in Figure 2(b) where the radial shape of the crystal at the final time is presented. We can measure and calculate the height of crystals over time, which allows us to gather information about their growth dynamics. The top view gives another measure for the contact radius and allow to verify if the droplet is spherical (Figure 2(c)), and provides valuable information about the early formation of the crystal and dynamics during evaporation. The sediments at final evaporation time t_{F} shown in Figure 2(d) provide quantitative and qualitative data for the understanding of the evaporation process. More information can be found in [18].

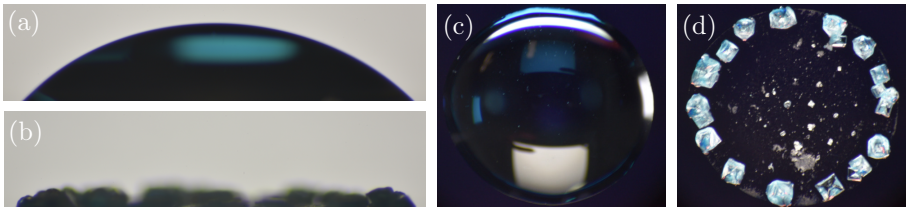

Figure 2: Side and top views of an evaporating sessile droplet of initial volume $V_0 = 10\ \mu$L with NaCl concentration of $1\,mol.L^{-1}$, and at relative humidity $RH = 0$ %. Side views at (a) initial time $t = 0$, and (b) final evaporation time t_{F}. Top views for the same droplet at (c) $t = 0$, and (d) t_{F}.

3. Results and Discussion

The fixed initial volume $V_0 = 10$ μL ensures that the Bond number is less than 1, which means that surface tension is dominant, and the droplet follows a spherical cap shape. The study initially focuses on the influence of salt concentration on the flow mechanisms and relates them to variations in surface tension with salt concentration. Later, the analysis shifts to the study of salt crystals, onset of crystal formation, and the influence of relative humidity on the final configuration. Finally, the study compares the final salt patterns for two high initial concentrations.

Influence of the salt concentration

This is a crucial point to ensure that the droplet evaporates in a pinned mode. When the initial salt concentration is too low, the droplet can evaporate in an unpinned mode, where the contact line recedes uniformly, and the droplet shape becomes flatter as it evaporates. In contrast, in the pinned mode, the contact line is anchored to the substrate, and the droplet shape can remain approximately spherical as it evaporates.

To study the impact of the initial salt concentration on the final pattern, the lowest concentration we choose still allows for the anchoring of the triple line during the full evaporation process. On the other hand, the maximum concentration is chosen to remain below the saturation value, which is the concentration above which no more salt can dissolve in the solvent. For sodium chloride in water, the saturation concentration is $c_{lim} = 6.1\ mol.L^{-1}$, which corresponds to a solubility of $36.0g/100g$ of water at $25\,^{\circ}$C and a molecular weight of $58.44\ g.mol^{-1}$ [19].

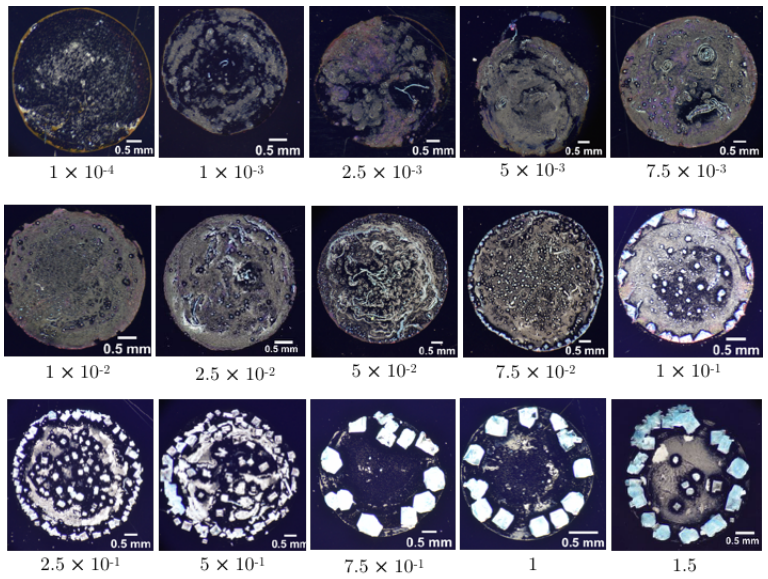

Figure 3: Final deposit patterns for several initial NaCl concentrations c_0 ranging from 10^{-4} to 1.5 $mol.L^{-1}$. Experimental conditions are : initial volume $V_0 = 10$ μL, relative humidity $RH = 10\%$ and controlled room temperature equal to 25.0 $^\circ$C.

Figure 3 shows the final patterns formed by the evaporating droplets for different initial salt concentrations c_0 ranging from 10^{-4} to 1.5 $mol.L^{-1}$. The experimental conditions are an initial volume of 10 μL, a relative humidity of 10%, and a controlled room temperature of 25.0 $^\circ$C.

When a droplet evaporates in a pinned mode, the liquid evaporating at the triple line is compensated by liquid coming from the center of the droplet, setting up a primary flow called capillary flow. The difference between the saturation vapor concentration near the evaporating interface c_{v_s} and the vapor concentration in the surrounding air c_{v_∞}, $\Delta c_v = c_{v_s} - c_{v_\infty} = c_{v_s}(1 - RH)$, is the driving mechanism of evaporation. The capillary flow J_c is proportional to the outgoing flow $J_v \sim f(\theta)\Delta c_v$, where $f(\theta)$ is a known

smooth function of the contact angle between 0 and 90 ° [20], therefore J_v mainly depends on the relative humidity RH [21].

The capillary flow brings all the salt present in the center of the droplet to the triple line during evaporation, as in the case of a pure water droplet evaporating in a pinned mode. At the triple line, salt accumulates, altering the surface tension and creating a gradient. The Marangoni flow induced by the surface tension gradient becomes important when the salt concentration is increased. This gradient drives a Marangoni flow that can transport salt towards the center of the droplet, where it can accumulate and eventually form crystals. Particle tracing and numerical simulations shows that the flow have only two components in the plane $z - r$, being respectively the vertical and radial directions, the flow is then symmetrycal around the z axis [9, 11].

The movement of the solute influences the surface tension, Figure 4 extracted from [3] shows the variation of surface tension with NaCl concentration. The experimental data for this curve were obtained from various references : the work of Jones and Ray [22] was used to characterize the called "capillary-inactive zone" for small NaCl concentrations, experimental data from Yizhak [23] provided also values for NaCl concentrations less than 1 $mol.L^{-1}$, while a publication by Markin et al. [24] was used for higher concentrations. We observe that the surface tension of the solution changes significantly as the salt concentration is increased beyond 10^{-2} $mol.L^{-1}$.

The Marangoni flow is given by $J_M \sim \frac{\partial \gamma}{\partial c} \Delta c$ [25]. Thus, the magnitude of the Marangoni flow is proportional to the gradient of the surface tension with respect to salt concentration and to the difference concentration $\Delta c = c - c_0$ where c_0 homogeneous initial concentration and c stand roughly by the edge

concentration which rise with time. Looking back at Figure 4, we can see that for a given initial concentration c_0, as the concentration at the edge of the drop increases with time, the local surface tension shifts to the right, the zone of high surface tensions. Solute conservation gives $cv = c_0V_0$, so the concentration at the edge of the drop increases as its volume decreases. As the drop is pinned, the decrease in volume is proportional to the decrease in drop height $h(t)$, and in the experiments in reference [18], equivalent to those shown in this publication, we observe that for the time it takes for the first crystals to appear, they have lost 80-90 % of their height, so the local concentration at the edge of the drop can increase by an order of magnitude to the right of the abscissa axis in Figure 4. This is the reason for the fairly wide transition zone.

The experimental results presented in Figure 3 show the influence of salt concentration on the final pattern observed after the droplet has fully evaporated. As the salt concentration is increased, we observe the formation of different patterns, ranging from a uniform deposit of salt crystals to more complex patterns with different shapes and symmetries. The variations in the final patterns can be related to the different hydrodynamic flows induced by the salt concentration and surface tension gradients, which can lead to different crystal nucleation and growth mechanisms.

The final salt deposit changes as the initial salt concentration increases, and patterns of salt crystals appear. We observe three different patterns: coffee-ring, uniform, and finite-size or crystal patterns.

For initial concentrations c_0 between $10^{-4}mol.L^{-1}$ and $10^{-3}mol.L^{-1}$, in the final deposit, there is always a coffee-ring pattern, where the solute is

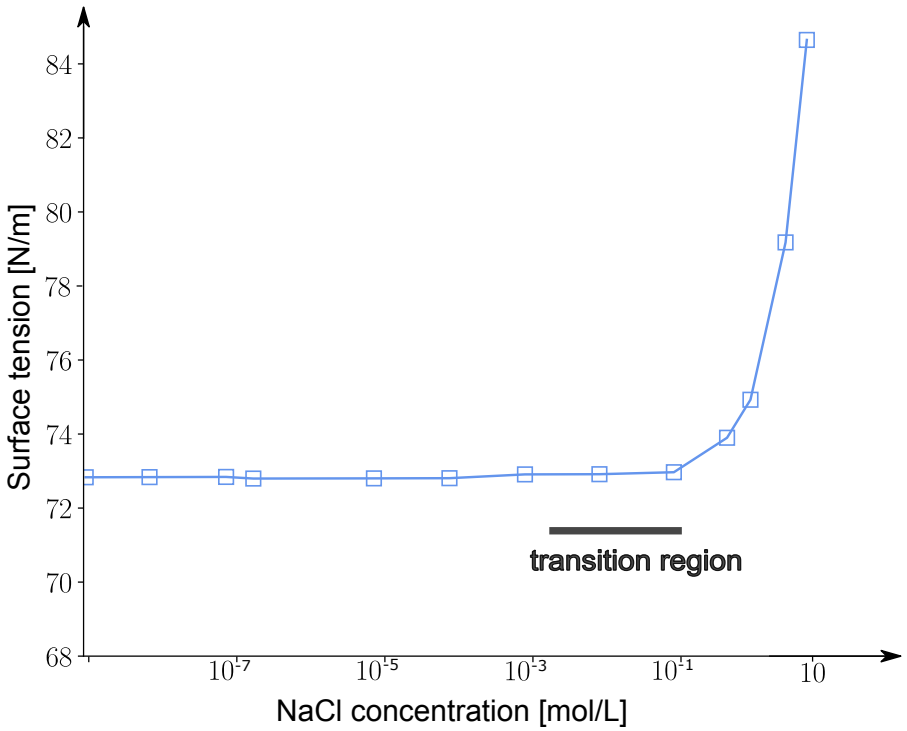

Figure 4: Surface tension as function of the NaCl concentration. From reference [3].

accumulated at the triple line and forms a ring. Coffee-ring deposits have been extensively studied, notably by Deegan [6, 26, 7] who first explained the hydrodynamics mechanisms behind the pattern formation.

In this regime, the variations of salt concentration are small, and the tension surface gradient is negligible $\frac{\partial \gamma}{\partial c} \sim 0$ (see Figure 4 below NaCl concentration of 10^{-3} $mol.L^{-1}$), and the main driving force is the differential evaporation flux at the triple line.

As schematized in Fig. 5(a), the balance flux is $J_c \geq J_M$, and the Marangoni flow only helps to carry the solute. The solute behaves as a passive tracer, not affecting the liquid properties, and their behavior is similar

to the behavior of colloids in droplets [27].

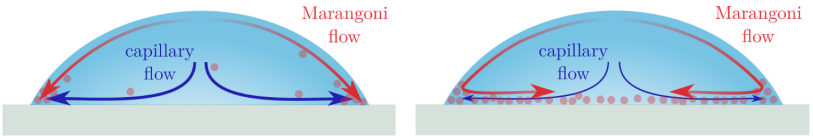

Figure 5: (a) Participation of the Marangoni flow in the formation of the coffee-ring pattern deposit. The Marangoni flow is low but transports solute to the triple contact line. (b) Formation of the uniform pattern. The quantity of liquid supplied at the contact line is too large compared to the evaporation flow so re-circulation cells appear.

By increasing the initial concentration c_0 recirculating cells appear in the droplet (see Fig. 5(b)) to ensure equilibrium and mass conservation at the triple line. We have a fluid flow back to the center of the droplet. The resulting deposit, therefore, does not form a pattern, but a thin layer of solute over the entire area initially occupied by the droplet. This is referred to as a uniform deposit (Fig 3) as it has already been observed in reference [7].

It is important to remember that the process happens in a series of steps, where the mechanisms happen one after the other. The geometry of the droplet and the pinned evaporation mode lead to capillary flow from the beginning of the evaporation, which transports the solute to the triple line. This locally increases the surface tension and causes a rise in surface tension. This second flow transports even more liquid and solute towards the edge of the droplet until recirculation cells are created. Here, both fluxes can be considered roughly equivalents.

Beyond $c_0 \sim 10^{-1}\ mol.L^{-1}$, the variations of the surface tension with the NaCl concentration are important as shown in Fig 4, and the Marangoni flow

dominates the internal flow, we have therefore $J_c \leq J_M$. Then to ensure mass conservation, the internal flow loses the azimuthal symmetry, and becomes three-dimensional and hydrodynamic stability appears along the droplet's edge. The non-homogeneous azimuthal flow develops zones of high salt concentration, called nodes, acting as an attractor giving a raise in the local salt concentration, and so the surface tension does. This azimuthal flow was already observed in [25] using a micron resolution Particle Image Velocimetry technique (micro-PIV). When the limit condition is reached finite salt crystals appear as observed on the triple contact line (Figure 3).

An analogy between temperature and salt concentration on the surface tension dependency is used to define a solutal Marangoni number Ma_s based on the thermal Marangoni number [28, 11, 29] ,

$$Ma_s = \frac{\partial \gamma}{\partial c} \frac{\Delta c \; r}{\mu D} \tag{1}$$

where γ is the surface tension, Δc is the difference of salt concentration, μ is the dynamic viscosity and D is the diffusion coefficient of the solute in the solvent. The critical solutal Marangoni number is around 10^2 according to literature [11, 20], and for higher values the Marangoni instability develops and forms recirculation cells. In a radial symmetry, the recirculation cell is characterized by a wavelength defined by the size of each cell. We think that at the end of the evaporation process, the distance between solid deposits is the same as the size of a cell.

The flows directed towards the forming crystals were observed in every direction using micro-PIV by Efstratiou et al [25], and the fact that the already formed crystals grow rather than new crystals are formed is justified by vortices localized in the crystals. A succession of well-distinct salt crys-

tals are what make up the solute deposit at the triple line, rather than a continuous salt ring.

The droplet radius in the experiments was $r = 2.15\ 10^{-3}m$, the dynamic viscosity $\mu = 10^{-3}Pa.s$ and the diffusion coefficient D is of the order of $10^{-5}m^2.s^{-1}$ [30]. The Marangoni number is around 10^3 for our experiments, which means that instabilities are always present, and triggered by the salt accumulation.

In the following we focus on Marangoni instabilities on experimental data, for concentrations c_0 above 1 $mol.L^{-1}$.

Crystals : onset and the influence of the relative humidity

The experimental configuration is a droplet of the initial volume $V_0 = 10\mu L$ with an initial concentration of $c_0 = 1\ mol.L^{-1}$ in a relative humidity $RH = 10\%$, and controlled temperature. We look for salt crystals during the evaporation process and call t_{1st} the time when they appear from the top view. At this time, the crystals' height is equal to the height of the droplet interface, and the first crystals appear. Figure 6 shows 6 time snapshots of the evaporation process starting from t_{1st} (first snapshot at 19 min 45 sec) every minute for 5 min.

In Figure 6 the drop is almost evaporated, the final time in this case is around 30 min, but difficult to assess precisely. We have repeated the experience for different relative humidity, $RH \in [20, 30, 40, 50\%]$ (not shown) and we recorded the time at which the crystals are visible on the top pictures. This time is scaled to the final time, which depends on the relative humidity. We find the first observable crystals at $t_{1st} = (65\pm6)\%$ of the final evaporation time t_f for all tested relative humidity. The result is consistent with those

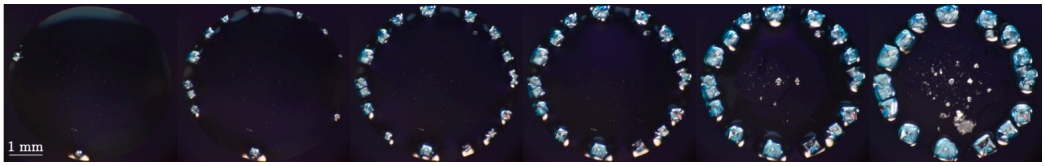

Figure 6: Top views of the evaporation dynamics of a sessile droplet of initial volume $V_0 = 10\ \mu L$ with 1 $mol.L^{-1}$ of NaCl at $RH = 10\%$. The formation of salt crystals is observed at the end of evaporation, from $t = 19\ min\ 45\ sec$ to $t = 24\ min\ 45\ sec$, every minute.

observed experimentally for micrometer sized droplets cited in [31].

As the droplet evaporates, more crystals appear around the perimeter of the droplet. We note that the position of the crystals does not change, and that the crystal growth is from the edge toward the center of the droplet. They also grow in height simultaneously. The Figure 7 shows the growth of the crystal in the perpendicular direction. The height of the data crystal is taken from the side image and is a function of t. The time when the maximum crystal height exceeds the maximal droplet height is defined as t^*.

The figure 7 presents three different experimental conditions as a function of NaCl concentration: one in the transition region (0.5 $mol.L^{-1}$), and two others in the Marangoni dominated region. In all situations, growth is linear, and we see a saturation at the maximum height for large initial concentrations.

The study of the deposits as a function of initial concentration and relative humidity shows that humidity does not seem to have an impact on the morphology of the salt deposit when the initial salt concentration is less than $c_0 = 10\ mol.L^{-1}$. But for higher concentrations, the pattern changes as the relative humidity increases, especially the size and arrangement of the salt

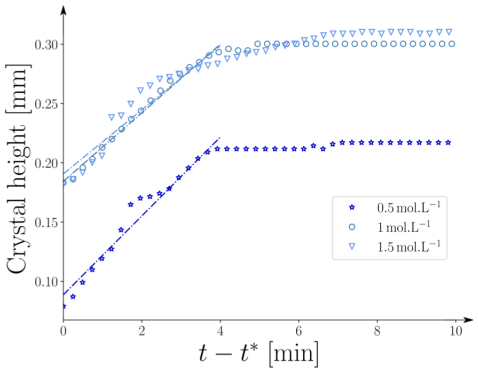

Figure 7: Crystal height as a function of time ($t^* - t$) for different initial salt concentrations, t^* is the time when the maximal crystal height exceeds the maximal droplet height. $V_0 = 10\mu L$ and $RH = 10\%$)

crystals.

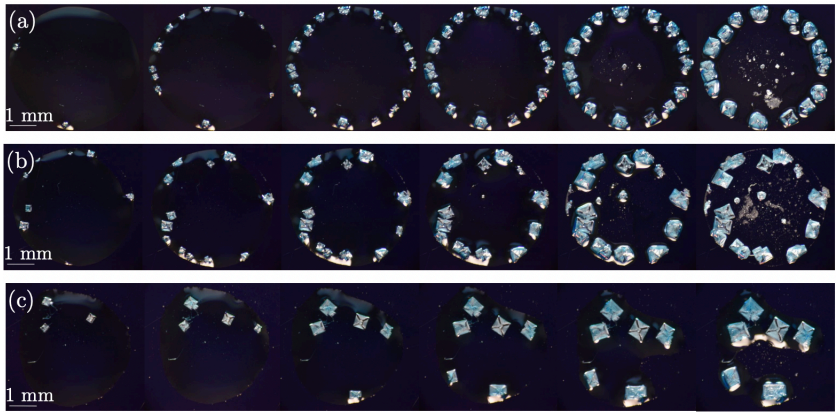

Figure 8: Top views of the evaporation dynamics an evaporating saline droplets for initial concentration $c_0 = 1\ mol.L^{-1}$ for different relative humidity : (a) $RH = 10\%$,(b) $RH = 30\%$ and (c) $RH = 50\%$.

285 Figure 8 presents the top view of an evaporating saline droplet for initial concentration of $c_0 = 1\ mol.L^{-1}$ for different relative humidity: (a) $RH =$

10%,(b) $RH = 30\%$ and (c) $RH = 50\%$. When the relative humidity is 10% or 30%, the crystals form exactly along the contact line and stick to the substrate right away. The crystals grow radially towards the center of the droplet without moving at all. This makes the contact line pinning stronger by making the substrate more wettable [32], and the contact line stays pinned until the end of evaporation. At the end of evaporation, the crystals are distributed along the triple contact line. For a higher relative humidity, $RH = 50\%$, the crystals are formed precisely at the contact line, but they do not adhere directly to the solid substrate and then are dragged towards the center. The inward displacement of the crystal during its growth is well explained in [33] using tension surface arguments, and it probably leads to the depinning of the contact line by modifying locally the internal flows [25]. The top part of the deposit is indeed pinning.

Crystals

We investigate the ordered crystal arrangement at the contact line, which is observed to be regular. Figure 8 illustrates that the distance between two adjacent crystals along the perimeter of the deposit is associated with the wavelength of the Marangoni instability. We quantify this distance λ as the average distance between two neighboring crystals over all the crystals present, such that $\lambda = \frac{1}{n}\sum_i \lambda_i$, where n denotes the number of crystals (see schema of figure 9).

On each last image of figure 8, the number of crystals decreases with RH, and the distance between crystals increases. There is a maximum amount of crystals that can be formed from the initial concentration of salt in the droplet since it is a fixed quantity. Based on the properties of the solute and

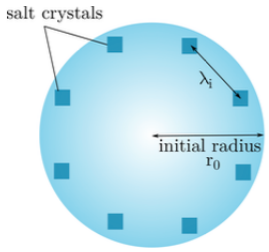

Figure 9: Schema of the measurements of the distance between two salt crystals in the final salt pattern. The distance λ is the average distance between the crystals $\lambda = \frac{1}{n}\sum_i \lambda_i$, where n is the number of crystals.

the solvent and the rate of evaporation, a maximal theoretical crystal yield can be calculated (see [34]) which gives the total mass of crystal.

We conducted several experiences for relative humidity between 10% and 50%, where the number of crystals and the distance apart between were measured on the final deposits. Over the range of humidity tested, the number of crystals was lower as long as the initial concentration c_0 increases. As with a given initial concentration, the number of crystals decreases as the humidity increases. Figure 10 shows the experimental values of $\frac{\lambda}{r_0}$ as a function of the relative humidity for initial concentrations of 1 and 1.5 $mol.L^{-1}$.

We assume that at the beginning of the process of evaporation, the concentration c_0 is homogeneous, and by using the conservation of solute $c_0V_0 = cV$, we can see that the concentration at the edge of the droplet is $c = c_0\frac{V_0}{V}$.

Now, the droplet volume V decreases linearly on time $\frac{V}{V_0} \sim (t_f - t)/t_f$ [21] therefore the concentration difference $\Delta c = c - c_0$ scales as $c_0\frac{t}{(t_f - t)}$, and

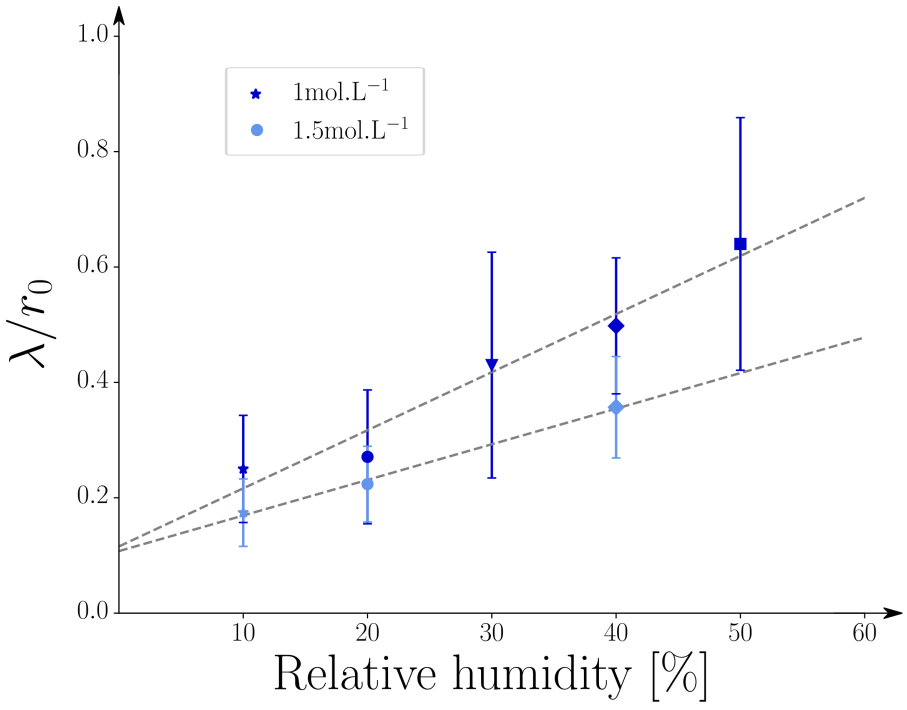

Figure 10: The averaged dimensionaless distance between crystals, $\frac{\lambda}{r_0}$, as a function of the relative humidity for initial concentrations of 1 and 1.5 $mol.L^{-1}$.

the solutal Marangoni number is now

$$Ma_s = \frac{\partial \gamma}{\partial c} \frac{r\ c_0 t}{\mu D(t_f - t)}.$$

Since the size of the Marangoni cells λ is inversely proportional to the square root of the Marangoni number $\lambda \sim Ma^{-1/2}$ [35, 36]. This means that an increase in the initial concentration c_0 will lead to smaller cells, as seen in Fig 10 for fixed relative humidity RH, and (ii) for a given initial concentration c_0 the rise of the humidity relative produces more long final time t_f resulting in large λ as in Fig 10 or equivalent less crystal deposits as in the last images of Fig 6 for (a) $RH = 10\%$,(b) $RH = 30\%$ and (c)$RH = 50\%$.

The coefficient λ appears to be finite and has a value of around 10% of the

initial radius for relative humidity tending to zero, but further experiments on very dry humidity are needed to assess this experimental approach.

4. Conclusions

In this study, we have investigated the impact of salt concentration on the dynamics of salt deposit formation. Our findings reveal two distinct regimes: the coffee-ring pattern, and the Marangoni-driven flow. Importantly, we have demonstrated for the first time the role of surface tension gradients, driven by changes in salt concentration, in inducing the Marangoni flow. Our proposed mechanism for solutal instability is in agreement with experimental observations and is consistent with previous studies in the literature.

The process of crystal sedimentation is proposed in two phases : the first phase extends from the initial time to 65 % of the evaporation time, during which we did not observe any significant crystal development, consistent with the literature. During the second phase, as local solute concentrations rise the Marangoni flow dominates, and the crystal arrangement is controlled by the wavelength of the Marangoni instability, which is related to the distance between two neighboring crystals at the perimeter of the deposit. Our findings suggest that the Marangoni instability is a crucial factor in determining the final salt deposit's crystal pattern, and it arises as a result of the relationship between surface tension and salt concentration. Our proposed mechanism for solutal instability is consistent with both the experimental results and the existing literature.

We define the normalized average distance between crystals in the second phase as a function of relative humidity and salt concentration, which pro-

vides quantitative data of the crystallization process. The number of crystals observed varies depending on relative humidity. As the relative humidity increases, the number of crystals obtained from the salt deposit will increase. The number of crystals is determined by the wavelength of the instability, which is proportional to the initial perturbation of the system. If the relative humidity is low, the evaporation flux will be strong, resulting in a high initial disturbance. The initial perturbation's value will determine the instability mode that will appear. A high perturbation gives a high instability mode with a small wavelength in the Marangoni cells.

A comprehensive investigation of the salt deposit formation after the complete evaporation of a sodium chloride-containing sessile droplet was carried out, yielding valuable insights into the intricate processes underlying the evaporation phenomenon. Our experimental findings support the solutal instability mechanism we proposed to account for the spatial arrangement of the salt crystals in the deposit.

References

[1] J. Park, J. Moon, Control of colloidal particle deposit patterns within picoliter droplets ejected by ink-jet printing, Langmuir 22 (8) (2006) 3506–3513.

[2] M. Kuang, L. Wang, Y. Song, Controllable printing droplets for high-resolution patterns, Advanced materials 26 (40) (2014) 6950–6958.

[3] V. Soulié, Sessile droplets of salt solutions on inert and metallic surfaces: influence of salt concentration gradients on evaporation and corrosion

behaviour, Ph.D. thesis, Université Montpellier; Universität Potsdam (2015).

[4] D. Brutin, B. Sobac, B. Loquet, J. Sampol, Pattern formation in drying drops of blood, Journal of fluid mechanics 667 (2011) 85–95.

[5] M. Parsa, S. Harmand, K. Sefiane, Mechanisms of pattern formation from dried sessile drops, Advances in colloid and interface science 254 (2018) 22–47.

[6] R. D. Deegan, O. Bakajin, T. F. Dupont, G. Huber, S. R. Nagel, T. A. Witten, Capillary flow as the cause of ring stains from dried liquid drops, Nature 389 (6653) (1997) 827–829.

[7] E. Bormashenko, Y. Bormashenko, R. Pogreb, O. Stanevsky, G. Whyman, Droplet behavior on flat and textured surfaces: Co-occurrence of deegan outward flow with marangoni solute instability, Journal of colloid and interface science 306 (1) (2007) 128–132.

[8] A. Edwards, P. Atkinson, C. Cheung, H. Liang, D. Fairhurst, F. Ouali, Density-driven flows in evaporating binary liquid droplets, Physical review letters 121 (18) (2018) 184501.

[9] H. Hu, R. G. Larson, Marangoni effect reverses coffee-ring depositions, The Journal of Physical Chemistry B 110 (14) (2006) 7090–7094.

[10] M. Majumder, C. S. Rendall, J. A. Eukel, J. Y. Wang, N. Behabtu, C. L. Pint, T.-Y. Liu, A. W. Orbaek, F. Mirri, J. Nam, et al., Overcoming the "coffee-stain" effect by compositional marangoni-flow-assisted drop-drying, The Journal of Physical Chemistry B 116 (22) (2012) 6536–6542.

[11] A. Darras, N. Vandewalle, G. Lumay, Transitional bulk-solutal marangoni instability in sessile drops, Physical Review E 98 (6) (2018) 062609.

[12] G. Xu, W. Hong, W. Sun, T. Wang, Z. Tong, Effect of salt concentration on the motion of particles near the substrate in drying sessile colloidal droplets, Langmuir 33 (3) (2017) 685–695.

[13] Y. Maruyama, K. Hasegawa, Evaporation and drying kinetics of water-nacl droplets via acoustic levitation, RSC advances 10 (4) (2020) 1870–1877.

[14] F.-I. Li, S. M. Thaler, P. H. Leo, J. A. Barnard, Dendrimer pattern formation in evaporating drops, The Journal of Physical Chemistry B 110 (51) (2006) 25838–25843.

[15] D. Brutin, Influence of relative humidity and nano-particle concentration on pattern formation and evaporation rate of pinned drying drops of nanofluids, Colloids and Surfaces A: Physicochemical and Engineering Aspects 429 (2013) 112–120.

[16] C. Diddens, Y. Li, D. Lohse, Competing marangoni and rayleigh convection in evaporating binary droplets, Journal of fluid mechanics 914 (2021) A23.

[17] V. Soulié, S. Karpitschka, F. Lequien, P. Prené, T. Zemb, H. Moehwald, H. Riegler, The evaporation behavior of sessile droplets from aqueous saline solutions, Physical Chemistry Chemical Physics 17 (34) (2015) 22296–22303.

[18] C. Lalanne, Evaporation of sessile droplets : hydrodynamics and salt deposit patterns, Theses, Sorbonne Université (Mar. 2022).
URL https://theses.hal.science/tel-03771836

[19] W. M. Haynes, Handbook of Chemistry and Physics, CRC Press LLC, 94th Edition.

[20] H. Hu, R. G. Larson, Evaporation of a sessile droplet on a substrate, The Journal of Physical Chemistry B 106 (6) (2002) 1334–1344.

[21] D. Brutin, Droplet wetting and evaporation: from pure to complex fluids, Academic Press, 2015.

[22] G. Jones, W. A. Ray, The surface tension of solutions of electrolytes as a function of the concentration. iii. sodium chloride, Journal of the American Chemical Society 63 (12) (1941) 3262–3263.

[23] Y. Marcus, Surface tension of aqueous electrolytes and ions, Journal of Chemical & Engineering Data 55 (9) (2010) 3641–3644.

[24] V. S. Markin, A. G. Volkov, Quantitative theory of surface tension and surface potential of aqueous solutions of electrolytes, The Journal of Physical Chemistry B 106 (45) (2002) 11810–11817.

[25] M. Efstratiou, J. Christy, K. Sefiane, Crystallization-driven flows within evaporating aqueous saline droplets, Langmuir 36 (18) (2020) 4995–5002.

[26] R. D. Deegan, O. Bakajin, T. F. Dupont, G. Huber, S. R. Nagel, T. A.

Witten, Contact line deposits in an evaporating drop, Physical review E 62 (1) (2000) 756.

[27] M. Anyfantakis, Z. Geng, M. Morel, S. Rudiuk, D. Baigl, Modulation of the coffee-ring effect in particle/surfactant mixtures: the importance of particle–interface interactions, Langmuir 31 (14) (2015) 4113–4120.

[28] D. Zang, S. Tarafdar, Y. Y. Tarasevich, M. D. Choudhury, T. Dutta, Evaporation of a droplet: From physics to applications, Physics Reports 804 (2019) 1–56.

[29] R. Bennacer, K. Sefiane, Vortices, dissipation and flow transition in volatile binary drops, Journal of fluid mechanics 749 (2014) 649–665.

[30] V. Vitagliano, P. A. Lyons, Diffusion coefficients for aqueous solutions of sodium chloride and barium chloride, Journal of the American Chemical Society 78 (8) (1956) 1549–1552.

[31] J. Ren, X. Zhong, L. Shen, F. Duan, Hydrodynamic pattern in drying saline droplet with suspended nanoparticles, Journal of Bionic Engineering 17 (4) (2020) 802–808.

[32] S. A. McBride, R. Skye, K. K. Varanasi, Differences between colloidal and crystalline evaporative deposits, Langmuir 36 (40) (2020) 11732–11741.

[33] N. Shahidzadeh, M. F. Schut, J. Desarnaud, M. Prat, D. Bonn, Salt stains from evaporating droplets, Scientific reports 5 (1) (2015) 1–9.

[34] J. W. Mullin, Crystallization, Elsevier, 2001.

[35] J. Pearson, On convection cells induced by surface tension, Journal of
470 fluid mechanics 4 (5) (1958) 489–500.

[36] V. X. Nguyen, K. J. Stebe, Patterning of small particles by a surfactant-enhanced marangoni-bénard instability, Physical Review Letters 88 (16) (2002) 164501.